Neonatal White Matter Damage Analysis Using DTI Super-Resolution and Multi-Modality Image Registration

Yi Wang *, Yuan Zhang[†], Chi Ma[‡], Rui Wang[§] and Zhe Guo [¶]
School of Electronics and Information
Northwestern Polytechnical University
1 Dongxiang Road, Chang'an District
Xi'an, Shaanxi 710129, P. R. China
wangyi79@nwpu.edu.cn
[†]*zhangyuan2000@mail.nwpu.edu.cn*
[‡]*13781637188@163.com*
[§]*wangrui2020@mail.nwpu.edu.cn*
[¶]*guozhe@nwpu.edu.cn*

Yu Shen
Henan Provincial People's Hospital, Henan Province No. 7 Weiwu
Henan 450000, P. R. China
hnsrmyyshenyu@163.com

Miaomiao Wang
The First Affiliated Hospital of Xi'an Jiaotong University
Xi'an, Shaanxi 710000, P. R. China
wangmm407@163.com

Hongying Meng
College of Engineering, Brunel University
Kingston Lane, Uxbridge, Middlesex, London, UB8 3PH, UK
Hongying.Meng@brunel.ac.uk

Punctate White Matter Damage (PWMD) is a common neonatal brain disease, which can easily cause neurological disorder and strongly affect life quality in terms of neuromotor and cognitive performance. Especially, at the neonatal stage, the best cure time can be easily missed because PWMD is not conducive to the diagnosis based on current existing methods. The lesion of PWMD is relatively straightforward on T1-weighted Magnetic Resonance Imaging (T1 MRI), showing semi-oval, cluster or linear high signals. Diffusion Tensor Magnetic Resonance Image (DT-MRI, referred to as DTI) is a noninvasive technique that can be used to study brain microstructures *in vivo*, and provide information on movement and cognition-related nerve fiber tracts. Therefore, a new method was proposed to use T1 MRI combined with DTI for better neonatal PWMD analysis based on DTI super-resolution and multi-modality image registration. First, after preprocessing, neonatal DTI super-resolution was performed with the three times B-spline interpolation

algorithm based on the Log-Euclidean space to improve DTIs' resolution to fit the T1 MRIs and facilitate nerve fiber tractography. Second, the symmetric diffeomorphic registration algorithm and inverse b0 image were selected for multi-modality image registration of DTI and T1 MRI. Finally, the 3D lesion models were combined with fiber tractography results to analyze and predict the degree of PWMD lesions affecting fiber tracts. Extensive experiments demonstrated the effectiveness and super performance of our proposed method. This streamlined technique can play an essential auxiliary role in diagnosing and treating neonatal PWMD.

Keywords: Punctate white matter damage; diffusion tensor magnetic resonance image (DTI); T1 MRI; nerve fiber tractography; DTI super-resolution.

1. Introduction

Punctate White Matter Damage (PWMD) is one of the most common white matter damages in preterm infants,[1–3] affecting the nervous system similar to Parkinson's Disease in adults.[4,5] Twenty-two percent of premature infants show PWMD, and the symptoms are cognitive, neuromotor or a visual impairment, and even develop into cerebral palsy in the later stages.[6] These symptoms are not evident in the neonatal period, so the best treatment period is easily missed. Therefore, converting undetectable clinical signs into quantifiable results to analyze and predict the development of PWMD by related medical image processing methods is crucial for disease treatment and neurodevelopment.

The lesion of PWMD is relatively clear on T1-weighted Magnetic Resonance Imaging (T1 MRI), showing the center of the semi-oval, lateral ventricle, cluster, or linear T1 high signals. Meanwhile, the cerebral white matter nerve fiber tracts from Diffusion Tensor Magnetic Resonance Imaging (DT-MRI, referred to as DTI) can be related to movement and cognition. The status of neonatal PWMD can be analyzed and predicted by the damage to nerve fiber tracts. Therefore, the image fusion technique of DTI and T1 MRI is used to research and analyze neonatal PWMD, combining the DTI tractography results with the lesions in T1 MRI. However, because the collection of neonatal DTI is more complex, the resolution is much lower than the T1 MRI, which is not conducive to the registration with the T1 MRI. And the DTI tractography results are not precise enough because the development of neonatal fiber tracts is incomplete. To solve the above-mentioned problems, the image super-resolution technique is used for DTI to improve the resolution and the tractography results.

Moreover, the fusion of DTI and T1 MRI is usually performed by image registration. But there are few methods of this multi-modality image registration since DTI is a tensor image, while T1 MRI is a scalar image. Therefore, a new streamline of neonatal PWMD analysis based on DTI super-resolution and multi-modality image registration is proposed.

DTI super-resolution algorithms can be divided into two categories. The first is the traditional tensor interpolation algorithm, and the other is the super-resolution method based on learning. Different from general scalar image interpolation, the tensor interpolation of DTI is much more complicated. Several tensor interpolation methods have been proposed. For example, tensor interpolation method based on tensor component form,[7] improved bilinear tensor interpolation method based on image grant features of the tensor field, and tensor interpolation method based on tensor eigenvalues and eigenvectors. These Euclidean space tensor interpolation methods can be calculated, but the swelling and nonpositive definite effects of the interpolated tensor may be caused.[8,9] The tensor interpolation method for medical images based on Riemann space[10] can avoid these defects, but the calculation is too complicated and takes a long time. In recent years, the development of super-resolution methods for medical images based on learning has been proposed more and more rapidly.[11–15] This kind of method has a good effect on general images. However, directly applying these networks to DTI tensors will also quickly cause the defects described above and cannot guarantee the consistency and the directions of the tensors. At the same time, the network's training model needs a large amount of data, which is hardly obtained.

There are also many technologies worth paying attention to in the problem of medical image overfraction. In 2009, Jiang *et al.*[16] proposed a method to achieve 3D high resolution diffusion Brain tensor image reconstruction of moving objects. In

2011, Estanislao *et al.*[17] presented a method for reconstructing diffusion-weighted MRI data on regular grids from scattered data. Next year, Benoit *et al.*[18] proposed a super-resolution reconstruction (SRR) technique for diffusion-weighted imaging (DWI) that overcomes limitations in spatial resolution by acquiring multiple anisotropic orthogonal scans and correcting for geometric distortions and patient motion. In 2019, Maria *et al.*[19] presented a novel method for higher order reconstruction of fetal diffusion MRI signal that enables detection of fiber crossings.

The tensor interpolation method based on Log-Euclidean space is a reasonable extension of the Riemann space interpolation method.[20,21] In Riemann space, the cone of a positive definite symmetric matrix is regarded as a standard and complete manifold; the swelling effect and nonpositive substantial effect can be overcome on this manifold, but the calculation is extensive. In 2004 and 2006, based on Riemann's space theory, Arsigny *et al.*[20,21] proposed DTI interpolation in Log-Euclidean space, which can also guarantee the constraint property of tensor and simplify the calculation in Riemannian space. In 2008, Fillard *et al.*[22] proposed a linear interpolation method based on Riemannian space. However, the interpolation process will damage the tensor anisotropy.[23] Therefore, since the tensor interpolation method based on Log-Euclidean space not only inherits the advantages of the Riemann space tensor interpolation algorithm but also significantly reduces the computational complexity, the B-spline tensor interpolation method based on Log-Euclidean space is chosen in this paper to eliminate swelling effect and nonpositive definite effect and also reduced computing time and complexity.

For the registration of DTIs and T1 MRIs, several registration methods of DTIs and T1 MRIs have been proposed. For example, Symmetric Diffeomorphic (referred to as Syn) registration of DTIs, T1 MRIs and Cerebral Blood Flow (referred to as CBF) MRIs,[24] and the registration of DTIs and T1 MRIs based on Mutual Information (referred to as MI), which uses DTIs as the constraint condition of T1 images in deformation tensor morphometry.[25] For other multi-modality image registration algorithms,[26] there are DTI multi-channel image registration algorithms based on diffeomorphic demons registration (referred to as demons),[27] the registration algorithm of DTIs and fMRIs based on Large Deformation Diffeomorphic Metric Mapping (referred to as LDDMM),[28] learning rigid image registration of T1 and T2 MRIs with convolutional neural networks,[29] deep learning-based inter-modality image registration of MRI and Computed Tomography (CT) images supervised by intra-modality similarity,[30] an Adversarial Image Registration Network (AIR-Net) based on GANs to deal with inflexible registration of MRIs and transrectal ultrasound (TRUS) images,[31] a 3D nonrigid registration of PET and CT images based on unsupervised deep learning,[32] a translation-based unsupervised deformable image registration of CT and MRIs,[33] a geometry-consistent adversarial unsupervised multi-modality registration of T1 and T2 MRIs as well as MRI and CT.[34]

However, the methods using neural network need many image data as the training set. This paper's data set is too small to use a neural network as the registration method.

Meanwhile, these registration algorithms use Fractional Anisotropy (referred to as FA) images for image registration instead of other derivative images of DTI. Therefore, to compare which modality of DTI derivative image is better for the registration with T1 MRI, five derivative images of DTI (including FA, MD, MD-in, b0, b0-in) are tested in this paper. The best derivative image b0-in of DTI is selected as the multi-modality image registration algorithm needed.

In summary, a new streamline of neonatal PWMD analysis based on DTI super-resolution and multi-modality image registration is proposed in this paper. PWMD can be effectively analyzed in this way.

2. Method

The main flowchart of the whole pipeline is shown in Fig. 1. First, DWIs were pre-processed and DTIs were estimated. Second, the B-spline tensor interpolation method based on Log-Euclidean space was used for DTI super-resolution. Next, the Syn registration method was performed between the corresponding DTIs and T1 MRIs for each subject. The deformation fields obtained from the registration
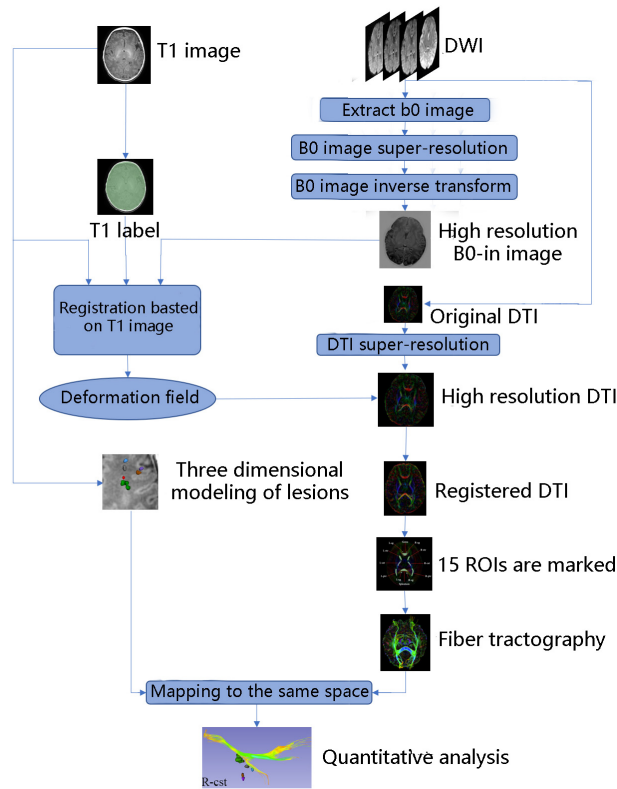
Fig. 1. Flowchart of the experiment. First, inverse b0 image derived from the super-resolved DTI is registered to the T1 image to obtain the deformation field, which acts on the super-resolved DTI. Then, fiber tractography is performed on registered DTI, and 3D lesions on T1 image are modeled. Finally, the fibers and the lesions are mapped to the same space for quantitative analysis.

were applied to the high-resolution DTIs by ANTs (http://stnava.github.io/ANTs/). Thus, the registered DTIs were generated and 15 corresponding regions of interest (ROIs) could be marked. Then, fiber tractography on each ROI was performed. Finally, 3D lesion models were drawn on T1 MRIs and combined with the fiber tracts to observe their spatial relationship.

2.1. *Materials*

Corresponding DTIs and T1 MRIs of 10 neonates with PWMD are from the Department of Radiology in the First Affiliated Hospital of Xi'an Jiaotong University in China. A GE 3.0T SignaHDxt MRI scanner was used. All the data are selected in good shape, free from motion artifacts. The specific scanning parameters of the DTI data are as follows: 30

gradient directions, b values are 0 and $600\,\mathrm{s/mm^2}$, TR = $11000\,\mathrm{ms}$, TE = $69.5\,\mathrm{ms}$, the layer thickness is $2.5\,\mathrm{mm}$, in-plane resolution of $0.703 \times 0.703\,\mathrm{mm^2}$, continuous scanning without gaps, Field of View (FOV) is $180 \times 180\,\mathrm{mm^2}$, the matrix is 128×128, resulting in the DTI resolution is $256 \times 256 \times 44$. For T1 MRIs, TR = $10.18\,\mathrm{ms}$, TE = $4.62\,\mathrm{ms}$, the in-plane resolution is $0.731 \times 0.731\,\mathrm{mm^2}$, the layer thickness is $1\,\mathrm{mm}$, continuous scanning without gaps, FOV = $240 \times 240\,\mathrm{mm^2}$, the matrix is 128×128, resulting in the T1 MRI resolution of $256 \times 256 \times 108$.

2.2. *Pre-processing*

In data preprocessing, the DWIs were performed with the correction of gradient field inconsistency and eddy current. After this, the skull portion in the image was removed, leaving only the brain tissue area, and the brain mask was calculated. These steps were completed by FSL (https://fsl.fmrib.ox.ac.uk/fsl/fslwiki/) with default parameters. Finally, tensor estimation was performed by DTI-TK (http://dti-tk.sourceforge.net/pmwiki/pmwiki.php) to obtain the DTI.

2.3. *DTI super-resolution*

Currently, widely used interpolation algorithms for DTI super-resolution are based on Euclidean space, which causes the swelling effect and nonpositive definite effect of the interpolation tensor.[35,36] Nonpositive actual effect: after interpolation, the eigenvalue of the interpolated tensor matrix may be zero or negative, which does not meet the requirement of positive-definite of the matrix. This effect will make it challenging to visualize tensor fields. Nonpositive definite tensor also has no real physical meaning in image processing. Swelling effect: in the Euclidean space, the interpolated tensor matrix, calculated by the weighted sum of two tensors, always has a larger matrix determinant than another tensor matrix. The swelling effect means that the dispersion of random variables corresponding to the interpolation tensor is larger than that of another tensor which is intuitively incompatible with physical meaning.

2.3.1. *DTI interpolation based on Riemann space*

Fillard[22] and Pennec[10] proposed a new metric that endows the tensor space with affine-invariant

Riemannian metrics to overcome this deficiency. It leads to strong theoretical properties: the positive definite symmetric matrices cone is replaced by a regular and complete manifold without boundaries (null eigenvalues are at infinity). In this metric, the interpolation tensor between two tensors is obtained by its linear interpolation on the shortest geodesic. For affine invariant metrics, the distance between a symmetric matrix with negative eigenvalues and zero eigenvalues and any tensor is infinite. Therefore, this method can avoid the appearance of nonpositive eigenvalues. Although the swelling effect and nonpositive definite effect are avoided, the amount of interpolation calculation required is much more than other methods.

2.3.2. *DTI interpolation based on Log-Euclidean space*

Arsigny *et al.*[20] proposed a Log-Euclidean space for tensor interpolation to overcome the computational constraints in Riemann space. This method transforms all the computations of tensor matrices into the calculation of vectors without any unnecessary complexity and dramatically reduces the computation. And it also can avoid the swelling effect and nonpositive definite effect. It is one of the most classical metrics in tensor computing.

2.3.3. *B-spline DTI interpolation based on Log-Euclidean space*

With the research of affine invariant metrics in Riemann space and Log-Euclidean space, more and more interpolation methods can be used for DTI interpolation. Barmpoutis *et al.*[37] extended the interpolation method of B-spline in vector value image to tensor image interpolation and proposed B-spline interpolation of tensor image based on Riemann metric.

Suppose there are N diffusion tensors on a one-dimensional grid $(\mathbf{D}_1, \mathbf{D}_2, \ldots, \mathbf{D}_N)$ and then interpolate between these N tensors. In linear interpolation, the interpolated point can be simply computed by computing the points on a geodesic connecting two continuous tensors. In higher dimensional space, a series of control points and node vectors are needed for interpolation. For B-spline interpolation in $k - 1$ times tensor space, there should be $N + k - 2$ control points $(\mathbf{A}_0, \mathbf{A}_1, \ldots, \mathbf{A}_{N+k-3})$ and $N + 2(k - 1)$ nodes

$(\mathbf{B}_{-k+1}, \mathbf{B}_{-k+1}, \ldots, \mathbf{B}_{N+k-2})$. For tensor $\mathbf{D}(u)$, $u \in [u_j, u_{j+1})$, B-spline interpolation based on Log-Euclidean space is chosen for DTI interpolation. B-spline curve equation in Log-Euclidean space is given by

$$\mathbf{D}(u) = \sum_{j=0}^{n} \tilde{\mathbf{A}}_j B_{j,k}(u). \tag{1}$$

$\tilde{\mathbf{A}}_j$ represents the control point tensor in Log-Euclidean space. In this space, cubic B-spline is chosen for DTI interpolation because cubic B-spline is precise enough and requires moderate computation. According to the properties of the B-spline curve, the cubic B-spline ($k = 3$) curve equation of tensor in Log-Euclidean space is given by

$$\mathbf{D}(u) = \exp\left(\frac{1}{6}(\,u^3 \quad u^2 \quad u \quad 1\,)\mathbf{M}_\alpha\left(\begin{pmatrix}\log(\mathbf{D}_0)\\\log(\mathbf{D}_1)\\\log(\mathbf{D}_2)\\\log(\mathbf{D}_3)\end{pmatrix}\right)\right), \tag{2}$$

$$\mathbf{M}_\alpha = \begin{pmatrix}-1 & 3 & -3 & 1\\3 & -6 & 3 & 0\\-3 & 0 & 3 & 0\\1 & 4 & 1 & 0\end{pmatrix}. \tag{3}$$

The B-spline curve in Log-Euclidean space is extended to the B-spline surface, and the B-spline surface equation of the two-dimensional tensor space is given by

$$\mathbf{D}(u,v) = \exp\left(\frac{1}{36}\begin{pmatrix}u^3\\u^2\\u\\1\end{pmatrix}^T \mathbf{M}_\alpha\right.$$
$$\times \begin{bmatrix}\log(\mathbf{D}_{0,0}) & \log(\mathbf{D}_{0,1}) & \log(\mathbf{D}_{0,2}) & \log(\mathbf{D}_{0,3})\\\log(\mathbf{D}_{1,0}) & \log(\mathbf{D}_{1,1}) & \log(\mathbf{D}_{1,2}) & \log(\mathbf{D}_{1,3})\\\log(\mathbf{D}_{2,0}) & \log(\mathbf{D}_{2,1}) & \log(\mathbf{D}_{2,2}) & \log(\mathbf{D}_{2,3})\\\log(\mathbf{D}_{3,0}) & \log(\mathbf{D}_{3,1}) & \log(\mathbf{D}_{3,2}) & \log(\mathbf{D}_{3,3})\end{bmatrix}$$
$$\left.\times \mathbf{M}_\alpha^T\begin{pmatrix}v^3\\v^2\\v\\1\end{pmatrix}\right). \tag{4}$$

For the interlayer interpolation of DTI, cubic B-spline curve equations in Log-Euclidean space for DTI interpolation and the interpolated tensor can be

obtained by interpolating the four surrounding tensors. For the layer interpolation of DTI, cubic B-spline surface equations in Log-Euclidean space for DTI interpolation and the interpolated tensor can be obtained by the interpolation of the 16 surrounding tensors. Because of the high order continuity of the B-spline, unlike some other interpolation methods that can produce jagged or abrupt changes, B-splines of order n are continuous up to $n-1$ derivatives. This makes the resulting interpolation smooth and helps in eliminating n-frequency noise from the tensor image.

2.4. *Registration of DTI and T1 MRI*

T1 images are scalar images, while DTI images are tensor images. Registration of different modality images is complex. DTI derivative images are scalar images, so they can be selected for registration with T1 MRI. However, the registration results between different DTI derivative images and T1 MRI are normally different. It is still an open question on which DTI derivative image is the best for the registration of DTI and T1 images. FA image, Mean Diffusion (referred to as MD) image, and b0 image derived from DTI were chosen for DTI and T1 MRI registration in this paper. In the MD image and b0 image, cerebrospinal fluid shows a high signal and white color, which is the opposite of T1 MRI. Therefore, the MD image and b0 image were processed by inverse gray transformation, named MD-inverse (referred to as MD-in) image and b0-inverse (referred to as b0-in) image, which makes cerebrospinal fluid show low signal and gray color. After this processing, the MD-in image and b0-in image are similar to T1 MRI, so that they can be used for DTI and T1 MRI registration.

We selected six widely used scalar-based registration methods for comparative experiments. Affine registration,[38,39] Rigid registration,[40] B-spline registration,[41] Elastic registration,[42] Demons registration[43] and Syn[44] registration. And there were five kinds of DTI derivative images being used for registration as previously stated. The overlap rate and error rate were used to evaluate the registration results. Visual evaluation was used as an aid. Since the punctate lesion of PWMD is located on the T1 image, the location of the lesion needs to be accurate and cannot be changed. Therefore, in this paper,

the T1 MRIs were used as the fix images, and DTIs were registered to T1 images. The experimental procedure of the registration part is shown in Fig. 2. After the registration, a deformation field was obtained, which was then applied to the high-resolution DTI. Thus, a registered DTI could be obtained.

2.4.1. *T1 MRI mask making*

DTI mask can be generated automatically during DTI preprocessing. However, the neonatal brain is not fully developed, and there is no apparent separation between the brain tissue and the skull. In addition, the artifact of neonatal data collection is significant, resulting in the mask's low accuracy generated by neonatal T1 MRI. To generate a more accurate T1 MRI mask, T1 MRI was selected as the template to register the b0 image, and the generated deformation field was applied to the DTI mask to obtain a more accurate T1 MRI mask. This T1 MRI mask can be used as input in registration. Figure 3 shows the mask of two images.

2.4.2. *Evaluation metrics*

We selected two overlapping rates to evaluate the overall brain registration accuracy of multi-modality image registration. The quantitative indexes measure expressed as the degree of overlap between the
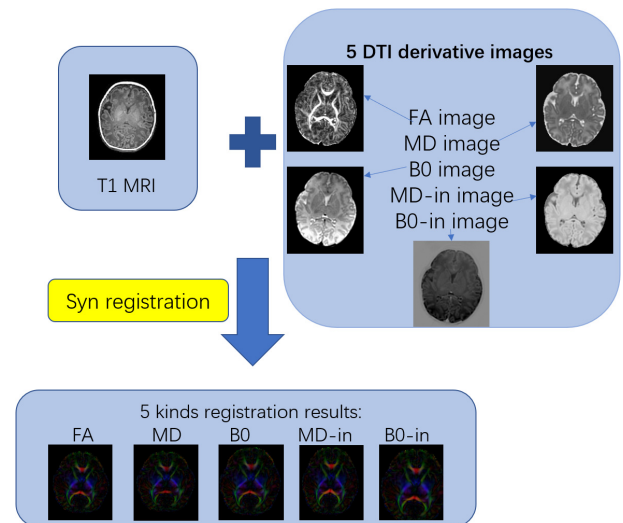

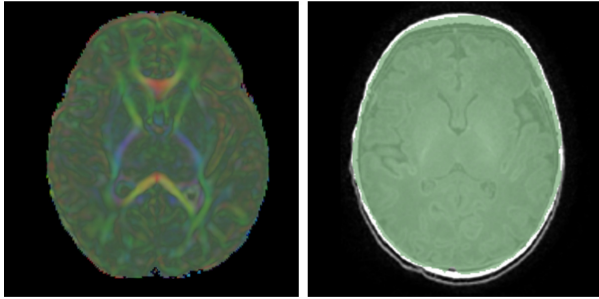Fig. 2. Syn registration algorithm and DTI derivative images.

Fig. 3. The DTI mask generated automatically is shown on the left, while the T1 MRI mask generated manually is shown on the right.

template image and the image volume after registration. The first quantitative index is Template Overlap (referred to as TO), which is defined as the volume of the overlapping region of the template image and the registered image divided by the volume of the template image. The larger the TO is, the better the registration result will be. The value range of TO is from 0 to 1, and a value closer to 1 indicates a better registration result. TO is given by

$$\text{TO} = \frac{\text{Tem} \bigcap \text{Mov}}{\text{Tem}}. \tag{5}$$

Tem represents the region in the template image, that is T1 MRI. Mov is the region in the registered image, that is registered DTI. Tem $\bigcap$ Mov represents the overlapping area of the template image and the image after registration.

The second quantitative index is Union Overlap (referred to as UO), defined as the overlapping area of the template image and the registered image divided by the union area of the template image and the registered image. The larger the UO is, the better the registration result will be. The value range of UO is from 0 to 1, and a value closer to 1 indicates a better registration result. UO is given by

$$\text{UO} = \frac{\text{Tem} \bigcap \text{Mov}}{\text{Tem} \bigcup \text{Mov}}. \tag{6}$$
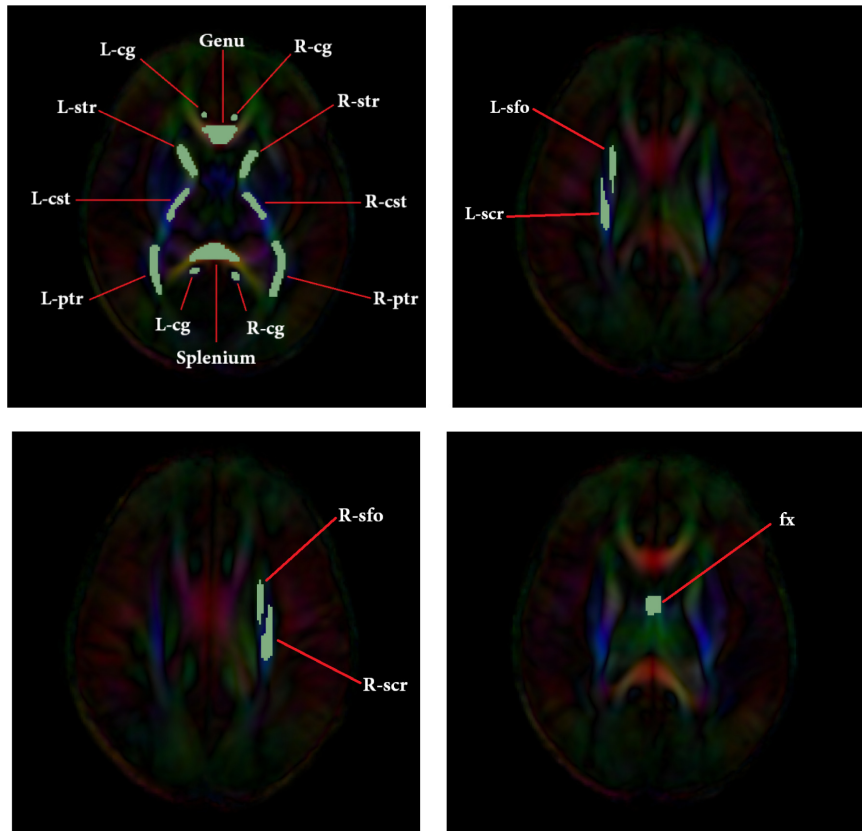

Fig. 4. (Color online) Neonatal DTI with 15 ROIs. The green part is the marked ROIs, and the names of ROIs are marked with red lines and white words.

To supplement the evaluation criteria in the above equations, false-negative errors (referred to as FNE) and False positive errors (FPE) are also calculated. FNE is a measure of the template image region incorrectly identified as a nontemplate image in registration. It is the region of the template image outside the registered image divided by the region of the template image. The smaller the FNE is, the better the registration result will be. The value range of FNE is from 0 to 1, and a value closer to 0 indicates a better registration result. FNE is given by

$$\text{FNE} = \frac{\text{Tem} \backslash \text{Mov}}{\text{Tem}}. \tag{7}$$

Tem\Mov represents the size of the part of the template image that does not overlap with the registered image.

FPE is a measure of the volume outside the template image that has been incorrectly identified as a template image which is defined as the volume outside the template image divided by the volume of the registered image. The value range of FPE is from 0 to 1, and a value closer to 0 indicates a better registration result. FPE is given by

$$\text{FPE} = \frac{\text{Mov} \backslash \text{Tem}}{\text{Mov}} \tag{8}$$

Mov\Tem represents the size of the part of the image that does not overlap with the template image after registration.

2.5. *15 ROIs*

There are about 15 ROIs in DTI associated with PWMD, namely genu, splenium, bilateral cingulum (referred to as cg), bilateral corticospinal tract (referred to as cst), bilateral superior thalamic radiation (referred to as str), bilateral posterior thalamic radiation (referred to as ptr), superior bilateral fasciculi fronto-occipitalis (referred to as sfo) and brain fornix (referred to as fx), superior corona radiata (referred to scr). The 15 ROIs were drawn manually by 3D Slicer (http://www.slicer.org/) as shown in Fig. 4.

3. Experiments

3.1. *DTI super-resolution*

To compare the difference between original DTI and interpolated DTI to evaluate the effect of the interpolation method, the original DTI with the resolution of $256 \times 256 \times 44$ was resampled to the DTI with the resolution of $128 \times 128 \times 30$ first. And then, the resampled DTI was interpolated by a different tensor interpolation method to obtain the new restored DTI with the resolution of $256 \times 256 \times 44$. The resolution of both original DTI and interpolated DTI were $256 \times 256 \times 44$, so they can be compared to evaluate different tensor interpolation methods. The interpolated results of the four methods are shown in Fig. 5. Four interpolation methods were tested, including Linear interpolation based on Euclidean space (EU-L), B-spline interpolation based on Euclidean space (EU-B), Linear interpolation based on Log-Euclidean space (LE-L) and B-spline interpolation based on Log-Euclidean space (LE-B).

It can be seen from Fig. 5 that the DTI edge becomes rough after the down-sampling, and each part is jagged due to the reduction of resolution. Four different interpolation methods were used to interpolate the DTI after the reduction of sampling. The DTI edge of EU-L DTI is fuzzy and jagged. In EU-B DTI, a series of error interpolation tensor points appear outside DTI, but the other part is smooth. In LE-L DTI, the interpolated edge is smoother, but each part still has some serration. In LE-B DTI, the interpolated edge and each part in DTI are relatively smooth, and there is no problem with many false interpolation tensor points in EU-B.

The genu in interpolated DTI was magnified for observation, as shown in Fig. 6. It can be seen that the genu of down-sampling DTI becomes fuzzy and jagged. The genu in EU-L and LE-L DTI are still relatively fuzzy, and the optimization effect of interpolation is very low compared with the down-sampling DTI. The genu in EU-B and LE-B DTI are relatively clear and smooth, which is very close to genu in original DTI. Therefore, the effect of the B-spline interpolation method based on Log-Euclidean space is the best.

The DTI fiber tractography results in different ROIs are the focus of this paper, so the fiber tractography results of genu, splenium, str and ptr before and after interpolation in 10 subjects are selected. The average FA values of 10 subjects of DTI fiber tractography results are calculated and shown in Table 1. The best results on each column in the table are shown in bold.
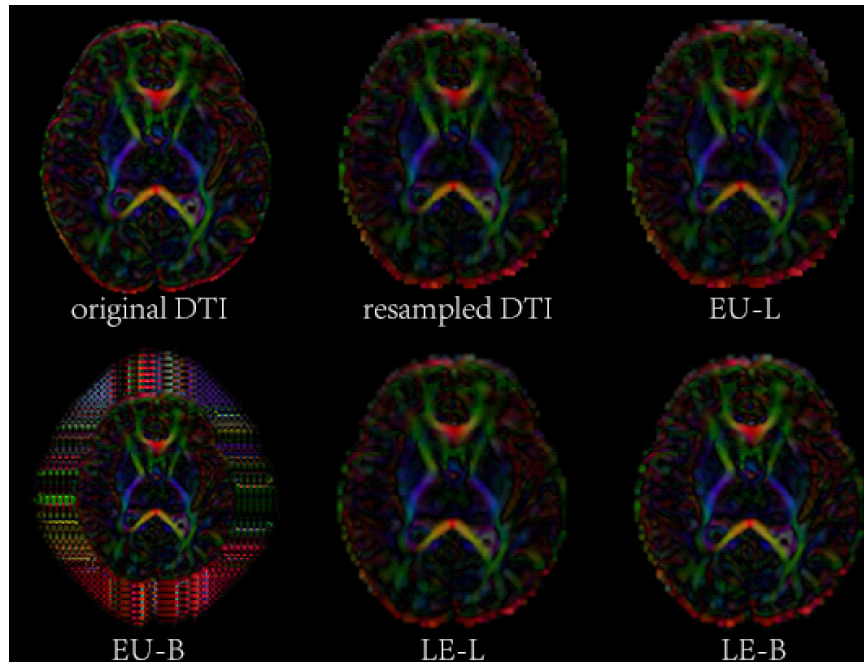
Fig. 5.   (Color online) Four interpolation results of EU-L, EU-B, LE-L and LE-B. (The color of DTI is encoded according to the principal eigenvectors direction of each tensor in the manner that follows the default setting of 3D Slicer. Red represents left and right direction; Green represents anterior and posterior direction; Blue represents superior and inferior direction.)

It can be seen from Table 1, the FA values of DTI fiber tractography results of EU-L and LE-L are significantly decreased. The FA values of DTI fiber tractography results of EU-B and LE-B decrease less, and LE-B is the closest to the original data on the whole. Therefore, the anisotropy of interpolated DTI is well maintained with LE-B.
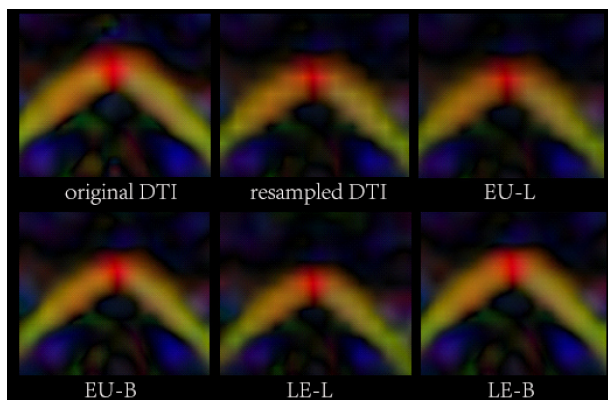

Fig. 6.   Genu in four interpolated DTIs. The first one is original DTI, the second one is resample DTI, the last four pictures show four different interpolation results.

Three kinds of DTI derivative images, FA image, Mode image and RA image, were chosen to analyze the derivative images of interpolated DTI and original DTI by the Mean Square Error (MSE). MSE represents the mean of the sum of squares of errors at the corresponding points between the interpolated DTI and the original DTI. The results are shown in Table 2. The best results on each column in the table are shown in bold.

The smaller is the MSE, the smaller the difference between the interpolated DTI and the original DTI will be. It can be seen from Table 2, the interpolated results of LE-B were the best on the whole, and the interpolated results of EU-B were the worst.

The above interpolation operation is to interpolate the down-sampling DTI to the same resolution as the original DTI. The only purpose is to evaluate and analyze the interpolation algorithm by comparing the difference between the original DTI and the interpolated DTI, and the conclusion is that B-spline tensor interpolation based on Log-Euclidean space is the best. However, this paper aims to interpolate the original DTI to the same resolution as T1 MRI. After interpolation, the DTI resolution was greatly

Table 1. The average FA values of interpolated DTI fiber tracts.

	splenium	genu	str	ptr
original	0.4785	0.3970	0.2832	0.3394
EU-L	0.4047	0.3434	0.2410	0.2886
EU-B	**0.4651**	0.3732	0.2649	0.3241
LE-L	0.4201	0.3439	0.2299	0.3001
LE-B	0.4607	**0.3797**	**0.2694**	**0.3260**

improved, and the fiber tractography results were optimized.

The resolution of original DTI was $256 \times 256 \times 44$. It was low, and the fiber tractography result was poor. After the above analysis, the B-spline interpolation method based on Log-Euclidean space was selected to interpolate the original DTI, and the resolution of interpolated DTI was increased to $256 \times 256 \times 108$ as the resolution of T1 MRIs.

Splenium, genu, str and ptr were selected as examples. The streamlined fiber tracking was also performed by 3D Slicer. The fiber tractography results of original DTI and interpolated DTI were used to compare the changes. The fiber tractography results of healthy adults were provided as a reference. The results are shown in Fig. 7.

It can be seen that the fiber tractography results of DTI interpolated by B-spline interpolation method based on Log-Euclidean space was optimized, which is close to the fiber tractography results of DTI adult, especially splenium and ptr.

3.2. *Registration of DTI and T1 MRI*

The registration results between five super-resolved DTI-derived images (b0, FA, MD, b0-in, MD-in images) and T1 MRI are shown separately in Fig. 8. From b0 image and FA image registration results, it can be seen that genu is almost invisible on the same slice. For MD image, MD-in image and b0-in image

Table 2. MSE comparison of interpolated DTI and original DTI.

	FA	Mode	RA
EU-L	0.0049	0.0496	**0.0011**
EU-B	0.0406	0.0583	0.0239
LE-L	0.0033	0.0445	0.0076
LE-B	**0.0032**	**0.0386**	0.0068

registration results, genu was clearer on the same slice. Therefore, it can be seen that the registration results of the MD, MD-in and b0-in images were better than those of the b0 and FA images, among which the results of the FA image were the worst.

However, all the subjects in this study were neonates with suspected PWMD. Because neonatal brain development is incomplete, and the white matter fiber bundles are thin and do not have completely myelin, most of the multi-modality image registration evaluation criteria are only applied to adult DTI data. Therefore, in this paper, TO, UO, FNE and FPE of the registered DTI and T1 images were selected to evaluate the results of multi-modality image registration.

In this experiment, 5 DTI derived images and 6 different registration algorithms were used for the registration of 10 newborn subjects. And the TO, UO, FNE and FPE of registration results were averaged to evaluate the registration results. The results are shown in Table 3–6.

The best results on the horizontal axis in each table are shown in bold and the best values on the vertical axis were underlined. From the results, it can be found that the Syn algorithm had the largest number of optimal values (i.e. values marked with underline). Additionally, the b0-in images had the largest number of optimal values (i.e. values highlighted in bold). Although not every metric in this combination was optimal, there was no other combination that outperforms this combination overall.

In summary, the best derived image was b0-in image, and the best registration algorithm was Syn algorithm. Therefore, b0-in image and Syn registration algorithm were used for the registration of T1 MRI and DTI in this paper. T1 MRIs was taken as templates, and the corresponding T1 mask was calculated. The b0-in image was used for registration. The deformation field was applied to the original interpolated DTI, and the tensor was reoriented to obtain the final registered DTI. The results are shown in Fig. 9. From left to right: T1 MRI, b0-in, and the final registered DTI.

3.3. *Neonatal PWMD analysis*

3.3.1. *T1 MRI lesion model construction*

In the case of one neonatal T1 MRI suspected to have PWMD, refer to Fig. 10, which includes
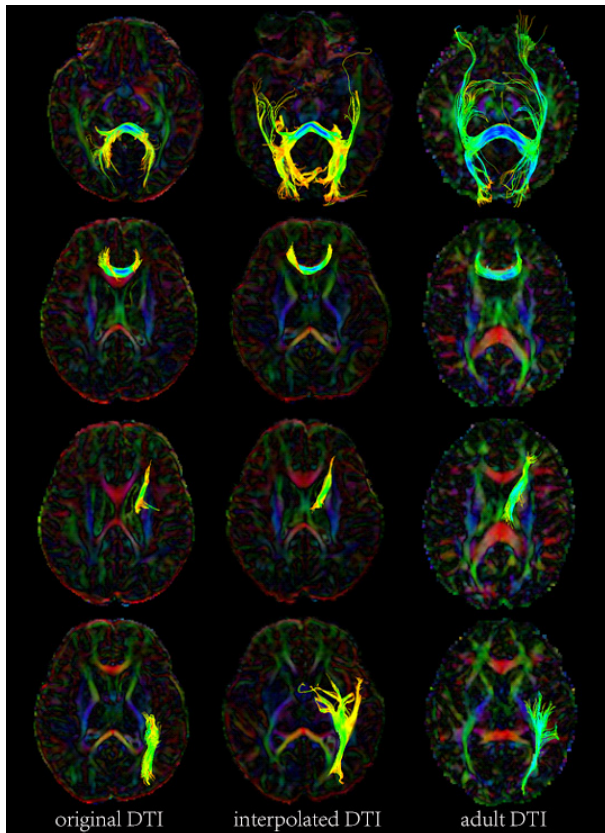
Fig. 7. (Color online) The nerve fiber tractography results of original DTI, interpolated DTI, and adult DTI. The images from top to bottom are genu, splenium, str and ptr. (Different from the color encoding of DTIs, the color of the fiber bundle is encoded according to the FA value in the manner that also follows the default setting of 3D Slicer. The closer the color is to blue, the larger the FA value.)

two different T1 MRI images. The lesions on T1 MRI were sketched manually, and the three-dimensional model of the lesions was constructed, as shown in Fig. 11. For the convenience of analysis and observation, the 3D model of the lesion can be divided into six parts for analysis as shown in Fig. 12. The 3D model of the lesion was analyzed with the results shown in Table 7.

3.3.2. *Fiber tractography results and PWMD analysis*

The DTIs (interpolated and registered previously) and generated 15 ROIs were used for fiber tractography. In addition, the fiber tracts were combined with the 3D lesion model generated above, and the

position relationship was observed and analyzed, as shown in Fig. 13.

It can be seen that the fiber tracts of r-ptr, r-sfo, r-scr, r-cst and r-str were close to the lesion model, where r-scr, r-sfo and r-cst intersect with the lesion. The degree of fiber tract damage with PWMD can be estimated from the proportion of fiber tracts affected by the PWMD lesion model to total fiber tracts, and the results are shown in Table 8.

4. Discussion

In this paper, a new streamline technique of neonatal PWMD analysis based on DTI interpolation and multi-modality image registration was proposed. The algorithms included B-spline interpolation based on Log-Euclidean space, multi-modality image registration of DTI and T1 MRI, and analysis of the influence of PWMD lesion on fiber tracts. DTI interpolation and multi-modality registration algorithm were effective and may predict and analyze PWMD. The entire algorithmic process takes only several minutes on a general-used computer.

PWMD is one of the most common white matter damages. Therefore, converting undetectable clinical symptoms into quantifiable results to analyze and predict PWMD using related medical image processing methods is crucial for disease treatment, neurodevelopment, and possible future methods.

Because the acquisition of neonatal DTI is complex, the resolution is much lower than T1 MRI, which is not conducive to the registration of T1 images, and the development of neonatal white matter nerve fiber tracts is not complete; the obtained results of fiber tractography are poor. To solve this problem, the super-resolution method can be adopted for neonatal DTI to improve the resolution of DTI, facilitate the realization of registration, and help improve the results of DTI fiber tractography. In addition, T1 images need to be registered with DTI to fuse the lesions in T1 images with the nerve fiber tracts of DTI; since DTI is a tensor image and T1 images are scalar images, the registration is complex because the DTI has a variety of scalar derivative images that can be used with T1 image registration.

Therefore, a new method was proposed to analyze neonatal white matter injury based on DTI

(a) registration with b0 (b) registration with FA (c) registration with MD

(d) registration with b0-in (e) registration with MD-in
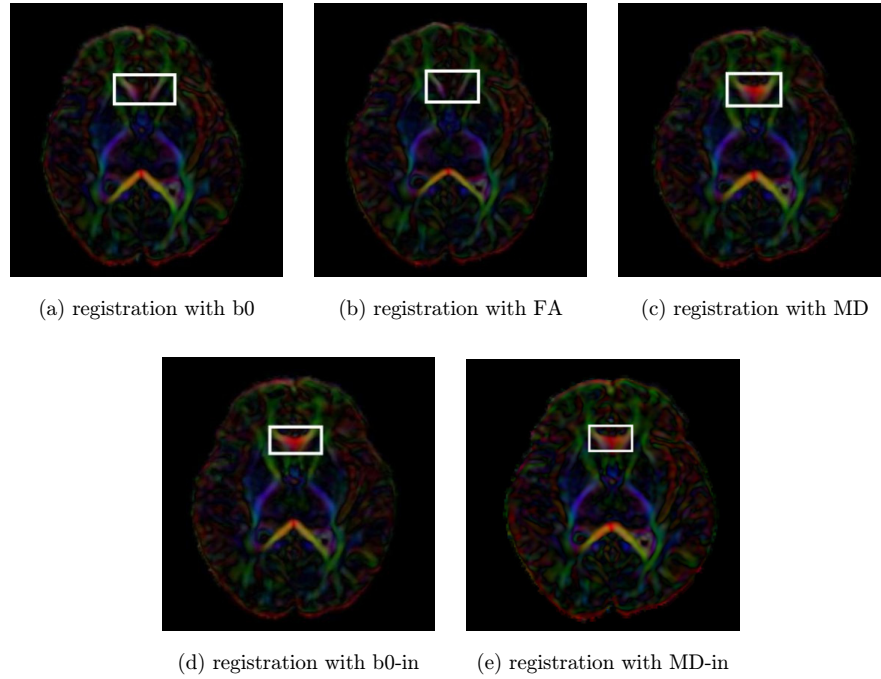
Fig. 8.   Registration results between five DTI-derived images and T1 MRIs with Syn algorithm in the same slice; the white box is the region of genu.

Table 3.   The TO average.

	FA	MD	MD-in	b0	b0-in
Affine	0.8691	0.8829	0.8875	0.8842	**0.8976**
Rigid	0.8827	0.8931	0.8904	0.8918	**0.8969**
Bspline	0.8717	0.8981	0.9052	0.8868	**0.9073**
Elastic	0.8885	0.8976	0.9109	0.8905	**0.9117**
Demons	0.8834	0.8954	**0.9099**	0.8897	0.9047
Syn	<u>0.8950</u>	<u>0.9185</u>	**<u>0.9310</u>**	<u>0.9098</u>	<u>0.9284</u>

Table 5.   The FNE average.

	FA	MD	MD-in	b0	b0-in
Affine	0.1182	0.1003	0.1012	0.1186	**0.0979**
Rigid	0.1161	0.1048	0.1027	0.1165	**0.0968**
Bspline	<u>0.0822</u>	0.0939	0.0924	0.0852	0.0853
Elastic	0.0924	0.0826	0.0806	0.0823	**0.0738**
Demons	0.0969	0.0804	0.0809	0.0880	**0.0795**
Syn	0.0918	<u>0.0692</u>	<u>0.0686</u>	<u>0.0717</u>	**<u>0.0685</u>**

Table 4.   The UO average.

	FA	MD	MD-in	b0	b0-in
Affine	0.8240	**0.8412**	0.8384	0.8339	0.8402
Rigid	0.8175	<u>0.8420</u>	0.8410	0.8303	**0.8445**
Bspline	0.8283	0.8399	0.8438	0.8350	**0.8464**
Elastic	0.8304	0.8412	**0.8444**	0.8316	0.8440
Demons	0.8330	0.8373	0.8427	0.8303	**0.8452**
Syn	<u>0.8359</u>	0.8401	<u>0.8467</u>	<u>0.8381</u>	**<u>0.8469</u>**

Table 6.   The FPE average.

	FA	MD	MD-in	b0	b0-in
Affine	0.0989	0.1077	0.1091	0.1207	**0.0955**
Rigid	0.1005	0.1105	0.1119	0.1142	**0.0984**
Bspline	0.0986	<u>0.1034</u>	0.1048	0.1134	**0.0940**
Elastic	0.1000	0.1131	0.1074	<u>0.1090</u>	**0.0947**
Demons	<u>0.0977</u>	0.1068	0.1060	0.1115	**<u>0.0936</u>**
Syn	0.1008	0.1098	<u>0.1010</u>	0.1105	**0.0944**

super-resolution and multi-modal image registration. In this paper, a B-spline interpolation method based on Log-Euclidean space was implemented for neonatal DTI super-resolution, and the three times B-spline interpolation method of Euclidean space

was applied to Log-Euclidean space, which is suitable for tensor calculation. The interpolation method ensures the essential characteristics of the tensor, avoids the swelling effect and nonpositive definite effect of the interpolation tensor, and improves the
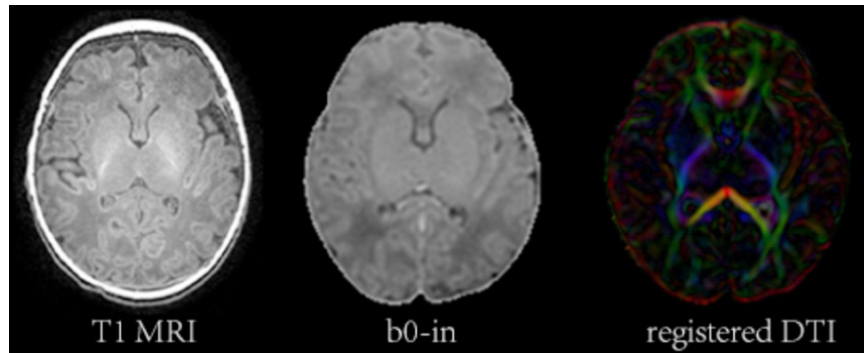
Fig. 9.   Registration results. The left two pictures show the T1 MRI and b0-in used in the registration process, and the third picture shows the registration result.
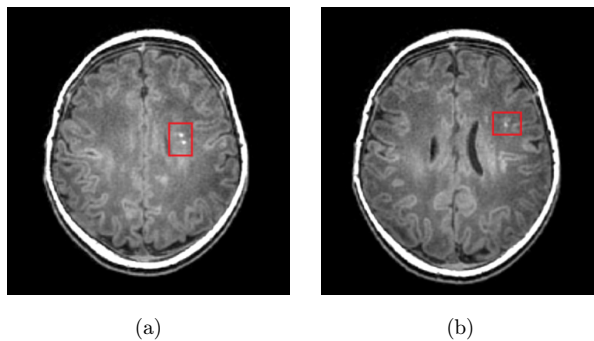

(a)   (b)

Fig. 10.   (Color online) Lesions in two different neonatal T1 MRI images. The lesions are in a red rectangle, which is very clear.

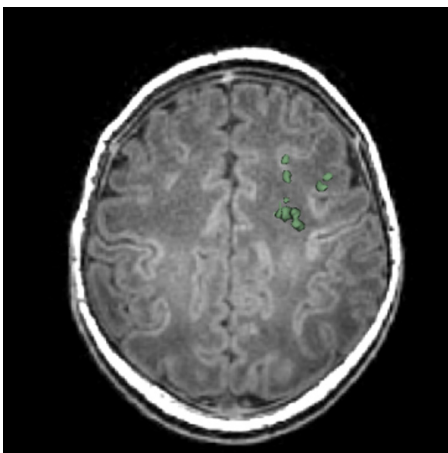tensor information of the neonatal DTI, making the results of nerve fiber tractography richer and more accurate.

Fig. 11.   (Color online) 3D model of lesions. The lesions were marked with green.

Subsequently, Syn registration method was used to register five derivative images of DTI (FA, MD, b0, MD-in, and b0-in images). The evaluation indexes based on vision and overlap rate were selected to evaluate the registration results. The results showed that the b0-in image had the best effect. Finally, the T1 MRI lesions were 3D modeled, and the neonatal DTI containing 15 ROIs was made and used for DTI fiber tractography.

By mapping the results of fiber tractography with the lesion model in the same space, the parameters of the lesion model and the degree of influence on the fiber tracts were calculated. And the damage situation of neonatal PWMD was analyzed, which can effectively be provided for the diagnosis and prediction of PWMD. Although the registration method used in this paper is the state of the art for the multimodality (DTI and T1 MRI) registration, errors cannot be completely avoided, which may affect the values of damage degree of fiber tracts, but will not affect much on what fiber tracts are close to the damages. The prediction of how the damages will affect the development of nervous system is mainly based on the closest fiber tracts instead of the damage degree.

In the experiment, it was found that some essential fiber tracts of the neonates had no myelin sheath and could not be displayed by interpolation, making the experimental results imperfect. Regarding registration, the effect of using the T2 image as the medium to register the T1 image with DTI should be the best. However, there is no T2 image in the data, so the registration results need improvement. Overall, according to the existing data and actual
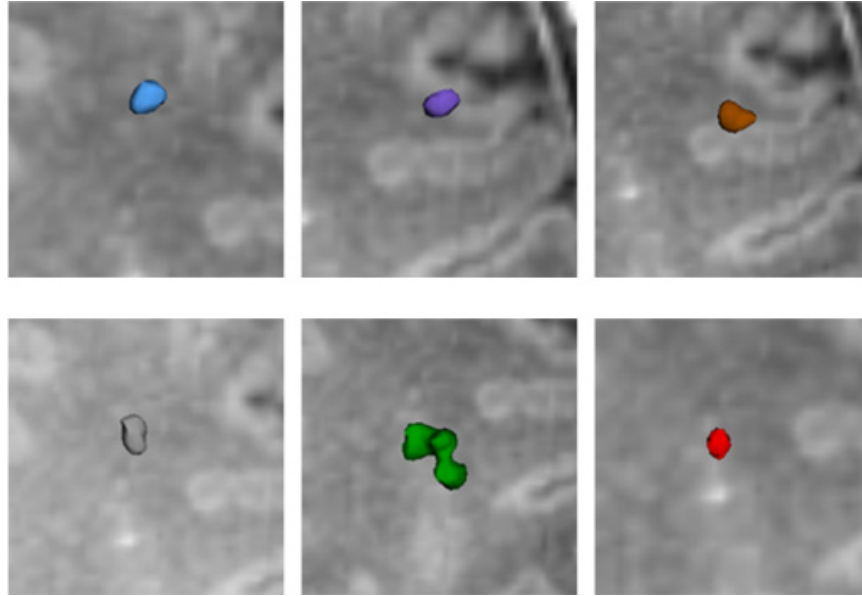
Fig. 12. (Color online) Six parts of the 3D lesion model. In each image, the lesions were marked with different colors to distinguish it from the surrounding grayscale image.

Table 7. The average FA values of interpolated DTI fiber tracts.

	a	b	c	d	e	f
slice	69-70	71-72	71-72	72-74	73-79	73-76
lesion superficial area (mm^2)	17.80	16.87	21.56	30.74	126.0	7.87
lesion volume (mm^3)	6.13	5.49	7.53	13.57	65.93	1.51

situation, the method in the paper can provide practical help for the early analysis of neonatal PWMD.

From Fig. 13 and Table 8, it can be inferred that the lesions have a great influence on the closest fiber tracts, e.g. r-sfo, r-scr and r-cst. Among them, r-cst and r-scr are projection fibers, which are ascending and descending fibers connecting cerebral cortex and subcortical structures. The main function of cst is autonomic movement control of the body and limbs, and r-cst damage may lead to movement disorder, limb paralysis and paraplegia in patients. At the same time, cst is also a projection fiber through the internal capsule. scr is the radial fibrous white matter between the internal capsule and the cerebral cortex. The internal capsule is one of the important structures in the cerebral hemispheres, and is where the projection fibers of the cerebral cortex link thalamus, brainstem, and spinal cord are dense.

Therefore, small lesions in the internal capsule area may cause serious obstacles to the movement and sensation of the contralateral half of the body. When hemorrhage or infarction occurs in this area of the neonatal, there may be loss of sensation of contralateral deflection in the future, spastic paralysis of the contralateral half of the body, and contralateral hemianopia in both eyes. When one side is damaged, the lesion contralateral lower limb is obviously clumsy. When walking, the patient often steps outward excessively. sfo is the association fibers between frontal lobe and occipital lobe. r-sfo is also influenced greatly by the lesions, so there may be some barriers in listening, speaking, reading and writing in this neonate. The above speculation about neonatal fiber bundle damage will be verified by following the patient's condition as much as possible in the future. This is an example of the PWMD analysis method based on the B-spline interpolation method
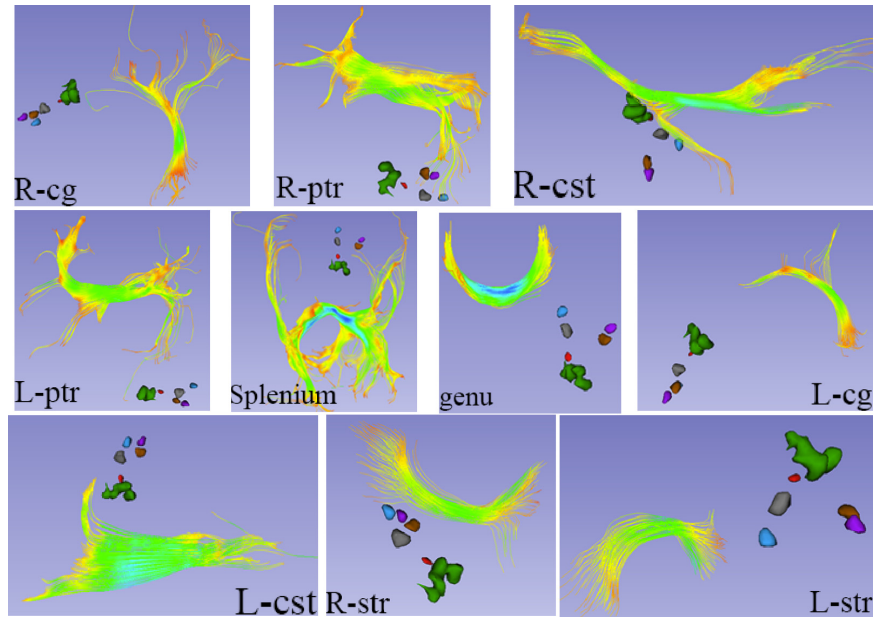
Fig. 13.   (Color online) Combined 3D lesion model with fiber tractography. The yellow green lines in the figure represent fiber bundles, and the irregular spheres in other colors represent lesions.

Table 8.   The damage degree of fiber tracts.

	Total	Damaged tracts	Damage degree
R-sfo	9	4	44.4%
R-scr	107	12	11.21%
R-cst	267	9	3.37%

in Log-Euclidean space and multi-modality registration algorithm for the analysis and prediction of neonatal PWMD, so as to better monitor, analyze, predict and diagnose related symptoms.

5. Conclusions and Future Directions

We propose a new streamline technique of neonatal PWMD analysis based on DTI super-resolution and multi-modality image registration. The three times B-spline interpolation based on the Log-Euclidean space was used for neonatal DTI super-resolution, improving its resolution and facilitating nerve fiber tractography. Syn registration algorithms and five DTI derivative images (FA, MD, b0, MD-in, and b0-in images) were selected for multi-modality image registration of DTI and T1 MRI. The results showed that the b0-in images were the best. The DTI and T1 MRI were registered using this method, 3D lesions model on T1 MRI was made, and the neonatal DTI with 15 ROIs was built for individual DTI fiber tractography results. The 3D lesion model was combined with fiber tractography results to analyze and predict the degree of PWMD lesion affecting nerve fiber tracts. This method may play an essential auxiliary role in diagnosing and treating neonatal PWMD.

Because the sample size used in this paper is too small to use deep learning-based method, a large number of data will be collected in the future, and then deep learning will be used as a further research direction.

Acknowledgments

ORCID

Yi Wang https://orcid.org/0000-0002-7743-1779

Zhe Guo ⬤ https://orcid.org/0000-0001-8024-1434

Miaomiao Wang ⬤ https://orcid.org/0000-0002-0852-8753

Hongying Meng ⬤ https://orcid.org/0000-0002-8836-1382

References

1. T. Niwa, L. S. de Vries, M. J. Benders, T. Takahara, P. G. Nikkels and F. Groenendaal, Punctate white matter lesions in infants: New insights using susceptibility-weighted imaging, *Neuroradiology* **53**(9) (2011) 669–679.

2. A. L. Nguyen, Y. Ding, S. Suffren, I. Londono, D. Luck and G. A. Lodygensky, The brains kryptonite: Overview of punctate white matter lesions in neonates, *Int. J. Dev. Neurosci.* **77** (2019) 77–88.

3. N. Tusor *et al.*, Punctate white matter lesions associated with altered brain development and adverse motor outcome in preterm infants, *Sci. Rep.* **7**(1) (2017) 1–9.

4. A. Gmez-Rodellar, J. Mekyska, P. Gmez-Vilda, L. Brabenec, P. Imko and I. Rektorov, A pilot study on the functional stability of phonation in EEG bands after repetitive transcranial magnetic stimulation in parkinsons disease, *Int. J. Neural Syst.* **33**(6) (2023) 2350028.

5. D. Gonzlez, R. Brua, J. C. Martnez-Castrillo, J. M. Lpez and G. De Arcas, First longitudinal study using binaural beats on parkinson disease, *Int. J. Neural Syst.* **33**(06) (2023) 2350027.

6. F. Arrigoni, D. Peruzzo, C. Gagliardi, C. Maghini, P. Colombo, F. S. Iammarrone, C. Pierpaoli, F. Triulzi and A. C. Turconi, Whole-brain DTI assessment of white matter damage in children with bilateral cerebral palsy: Evidence of involvement beyond the primary target of the anoxic insult, *Am. J. Neuroradiol.* **37**(7) (2016) 1347–1353.

7. L. Zhukov and A. H. Barr, Oriented tensor reconstruction: Tracing neural pathways from diffusion tensor MRI, in *IEEE Visualization 2002* (IEEE, 2002), pp. 387–394.

8. I. Hotz, J. Sreevalsan-Nair, H. Hagen and B. Hamann, Tensor field reconstruction based on eigenvector and eigenvalue interpolation, in *Scientific Visualization: Advanced Concepts*, Dagstuhl Follow-Ups (Schloss Dagstuhl–Leibniz-Zentrum fuer Informatik, 2010), pp. 111–123.

9. I. A. Yassine, High rank tensor and spherical harmonic models for diffusion MRI processing, PhD thesis, West Virginia University (2010).

10. X. Pennec, P. Fillard and N. Ayache, A Riemannian framework for tensor computing, *Int. J. Comput. Vis.* **66**(1) (2006) 41–66.

11. N. M. Elsaid and Y.-C. Wu, Super-resolution diffusion tensor imaging using SRCNN: A feasibility study, in *2019 41st Annual Int. Conf. IEEE Engineering in Medicine and Biology Society (EMBC)* (IEEE, 2019), pp. 2830–2834.

12. Q. Tian, Z. Li, Q. Fan, C. Ngamsombat, Y. Hu, C. Liao, F. Wang, K. Setsompop, J. R. Polimeni and B. Bilgic, SRDTI: Deep learning-based super-resolution for diffusion tensor MRI, preprint (2021), arXiv: 2102.09069.

13. T. A. Spears and P. T. Fletcher, Super-resolution of manifold-valued diffusion MRI refined by multi-modal imaging, in *Computational Diffusion MRI: 13th Int. Workshop, CDMRI 2022* (Springer, 2022), pp. 14–25.

14. U. Gimenez, J. C. Deloulme and H. Lahrech, Rapid microscopic 3d-diffusion tensor imaging fiber-tracking of mouse brain in vivo by super resolution reconstruction: Validation on map6-ko mouse model, *Magn. Reson. Mater. Phy.* **36** (2023) 577–587.

15. J. Zhu, C. Tan, J. Yang, G. Yang and P. Lio, Arbitrary scale super-resolution for medical images, *Int. J. Neural Syst.* **31**(10) (2021) 2150037.

16. S. Jiang, H. Xue, S. Counsell, M. Anjari, J. Allsop, M. Rutherford, D. Rueckert and J. V. Hajnal, Diffusion tensor imaging (DTI) of the brain in moving subjects: Application to in-utero fetal and ex-utero studies, *Magn. Reson. Med.* **62**(3) (2009) 645–655.

17. E. Oubel, M. Koob, C. Studholme, J.-L. Dietemann and F. Rousseau, Reconstruction of scattered data in fetal diffusion MRI, *Med. Image Anal.* **16**(1) (2012) 28–37.

18. B. Scherrer, A. Gholipour and S. K. Warfield, Super-resolution reconstruction to increase the spatial resolution of diffusion weighted images from orthogonal anisotropic acquisitions, *Med. Image Anal.* **16**(7) (2012) 1465–1476.

19. M. Deprez, A. Price, D. Christiaens, G. L. Estrin, L. Cordero-Grande, J. Hutter, A. Daducci, J.-D. Tournier, M. Rutherford and S. J. Counsell, Higher order spherical harmonics reconstruction of fetal diffusion MRI with intensity correction, *IEEE Trans. Med. Imaging* **39**(4) (2019) 1104–1113.

20. V. Arsigny, P. Fillard, X. Pennec and N. Ayache, Log-euclidean metrics for fast and simple calculus on diffusion tensors, *Magn. Reson. Med.* **56**(2) (2006) 411–421.

21. V. Arsigny, Processing data in lie groups: An algebraic approach. application to non-linear registration and diffusion tensor MRI, PhD thesis, cole Polytechnique (2004).

22. P. Fillard, Riemannian processing of tensors for diffusion MRI and computational anatomy of the brain, PhD thesis, Université Nice Sophia Antipolis (2008).

23. G. L. Kung, T. C. Nguyen, A. Itoh, S. Skare, N. B. Ingels Jr, D. C. Miller and D. B. Ennis, The presence of two local myocardial sheet populations confirmed by diffusion tensor MRI and histological validation, *J. Magn. Reson. Imaging* **34**(5) (2011) 1080–1091.

24. B. Avants, J. T. Duda, H. Zhang and J. C. Gee, Multivariate normalization with symmetric

diffeomorphisms for multivariate studies, in *Int. Conf. Medical Image Computing and Computer-Assisted Intervention* (Springer, 2007), pp. 359–366.

25. C. Studholme, Incorporating DTI data as a constraint in deformation tensor morphometry between T1 MR images, in *Biennial Int. Conf. Information Processing in Medical Imaging* (Springer, 2007), pp. 223–232.

26. A.-G. Legaz-Aparicio, R. Verd-Monedero, J. Larrey-Ruiz, J. Morales-Snchez, F. Lpez-Mir, V. Naranjo and A. Bernabu, Efficient variational approach to multi-modal registration of anatomical and functional intra-patient tumorous brain data, *Int. J. Neural Syst.* **27**(6) (2017) 1750014.

27. C. Tang, X. Xie and R. Du, Multi-modal image registration based on diffeomorphic demons algorithm, in *Fifth Int. Conf. Digital Image Processing (ICDIP 2013)* (SPIE, 2013), pp. 309–313.

28. M. I. Miller, M. F. Beg, C. Ceritoglu and C. Stark, Increasing the power of functional maps of the medial temporal lobe by using large deformation diffeomorphic metric mapping, *Proc. Natl. Acad. Sci. USA* **102**(27) (2005) 9685–9690.

29. J. M. Sloan, K. A. Goatman and J. P. Siebert, Learning rigid image registration-utilizing convolutional neural networks for medical image registration, in *Int. Joint Conf. Biomedical Engineering Systems and Technologies* (SCITEPRESS, 2018), pp. 89–99.

30. X. Cao, J. Yang, L. Wang, Z. Xue, Q. Wang and D. Shen, Deep learning based inter-modality image registration supervised by intra-modality similarity, in *Machine Learning in Medical Imaging: 9th Int. Workshop, MLMI 2018* (Springer International Publishing, 2018), pp. 55–63.

31. P. Yan, S. Xu, A. R. Rastinehad and B. J. Wood, Adversarial image registration with application for MR and TRUS image fusion, in *Machine Learning in Medical Imaging: 9th Int. Workshop, MLMI 2018* (Springer, 2018), pp. 197–204.

32. H. Yu, X. Zhou, H. Jiang, H. Kang, Z. Wang, T. Hara and H. Fujita, Learning 3d non-rigid deformation based on an unsupervised deep learning for PET/CT image registration, in *Medical Imaging 2019: Biomedical Applications in Molecular, Structural, and Functional Imaging*, Vol. 10953 (SPIE, 2019), pp. 439–444.

33. Z. Chen, J. Wei and R. Li, Unsupervised multi-modal medical image registration via discriminator-free image-to-image translation, preprint (2022), arXiv:2204.13656.

34. Y. Liu, W. Wang, Y. Li, H. Lai, S. Huang and X. Yang, Geometry-consistent adversarial registration model for unsupervised multi-modal medical image registration, *IEEE J. Biomed. Health Inform.* **27**(7) (2023) 3455–3466.

35. C. Dong, C. C. Loy, K. He and X. Tang, Learning a deep convolutional network for image super-resolution, in *Eur. Conf. Computer Vision* (Springer, 2014), pp. 184–199.

36. C. Ledig *et al.*, Photo-realistic single image super-resolution using a generative adversarial network, in *Proc. IEEE Conf. Computer Vision and Pattern Recognition* (IEEE, 2017), pp. 4681–4690.

37. A. Barmpoutis, B. C. Vemuri, T. M. Shepherd and J. R. Forder, Tensor splines for interpolation and approximation of DT-MRI with applications to segmentation of isolated rat hippocampi, *IEEE Trans. Med. Imaging* **26**(11) (2007) 1537–1546.

38. A. Leemans, J. Sijbers, S. De Backer, E. Vandervliet and P. M. Parizel, Affine coregistration of diffusion tensor magnetic resonance images using mutual information, in *Advanced Concepts for Intelligent Vision Systems: 7th Int. Conf., ACIVS 2005* (Springer, 2005), pp. 523–530.

39. D. Castillo-Barnes, C. Jimenez-Mesa, F. J. Martinez-Murcia, D. Salas-Gonzalez, J. Ramrez and J. M. Grriz, Quantifying differences between affine and nonlinear spatial normalization of FP-CIT spect images, *Int. J. Neural Syst.* **32**(5) (2022) 2250019.

40. C. Studholme, D. L. Hill and D. J. Hawkes, An overlap invariant entropy measure of 3d medical image alignment, *Pattern Recognit.* **32**(1) (1999) 71–86.

41. J. A. Schnabel, D. Rueckert, M. Quist, J. M. Blackall, A. D. Castellano-Smith, T. Hartkens, G. P. Penney, W. A. Hall, H. Liu and C. L. Truwit, A generic framework for non-rigid registration based on non-uniform multi-level free-form deformations, in *Medical Image Computing and Computer-Assisted Intervention MICCAI 2001: 4th Int. Conf.* (Springer, 2001), pp. 573–581.

42. D. C. Alexander and J. C. Gee, Elastic matching of diffusion tensor images, *Comput. Vis. Image Underst.* **77**(2) (2000) 233–250.

43. T. Vercauteren, X. Pennec, A. Perchant and N. Ayache, Diffeomorphic demons: Efficient non-parametric image registration, *NeuroImage* **45**(1) (2009) S61–S72.

44. B. Avants, J. T. Duda, H. Zhang and J. C. Gee, Multivariate normalization with symmetric diffeomorphisms for multivariate studies, in *Int. Conf. Medical Image Computing and Computer-Assisted Intervention* (Springer, 2007), pp. 359–366.